808 nm broad-area laser diodes designed for high efficiency at high-temperature operation

IOP Publishing Semiconductor Science and Technology
Semicond. Sci. Technol. **36** (2021) 105012 (11pp) https://doi.org/10.1088/1361-6641/ac2160

808 nm broad-area laser diodes designed for high efficiency at high-temperature operation

Yu Lan[1,2], Guowen Yang[1,2,3,*], Yuxian Liu[1,2], Yuliang Zhao[1,2], Zhenfu Wang[1], Te Li[1] and Abdullah Demir[4,*]

[1] State Key Laboratory of Transient Optics and Photonics, Xi'an Institute of Optics and Precision Mechanics, Chinese Academy of Sciences, Xi'an 710119, People's Republic of China
[2] University of Chinese Academy of Sciences, Beijing 100049, People's Republic of China
[3] Dogain Laser Technology (Suzhou) Co., Ltd, Suzhou 215123, People's Republic of China
[4] Bilkent University, UNAM—Institute of Materials Science and Nanotechnology, Ankara 06800, Turkey

E-mail: yangguowen@opt.ac.cn and abdullah.demir@unam.bilkent.edu.tr

Received 28 April 2021, revised 16 August 2021
Accepted for publication 26 August 2021
Published 21 September 2021

Abstract

Semiconductor lasers with high power conversion efficiency (PCE) and output power are heavily investigated driven by more energy-efficient commercial applications. In this paper, an asymmetric broad area laser (A-BAL) design is studied and compared with a conventional symmetric broad area laser (S-BAL) design for 808 nm single emitter laser diodes. We present a comparative theoretical and experimental investigation by studying the thermal effects on the laser parameters. The output characteristics and efficiency loss paths for the designs were analyzed. The leakage of carriers was identified as the primary source of the PCE reduction with temperature. Suppressing this leakage by optimization of the A-BAL design, a record continuous-wave PCE of 68% at 25 °C and 60.4% at 75 °C were achieved for a single emitter laser with 10 W output power. These devices deliver high efficiency at high temperatures with reliable operation achieving 2000 h of an accelerated aging lifetime without failures.

Keywords: semiconductor laser, laser diode, high power, high efficiency, 808 nm

(Some figures may appear in color only in the online journal)

1. Introduction

Laser diodes (LDs) at 808 nm are widely used in materials processing [1, 2], optically pumped solid-state lasers [3–5], and medical applications [6, 7]. The performance and reliability of diode lasers have been dramatically improved by the advancement in epitaxial growth technologies and the introduction of novel or optimized epitaxial designs [8–17]. In these applications, high power conversion efficiency (PCE) has been a key design parameter and performance indicator for LDs, which is defined as optical output power per input electrical power (i.e. $\eta_c = P_{out}/(IV)$). Higher PCE improves the laser output power, reduces the heat dissipation and cost, and allows smaller footprint of a laser system. Continuous wave (CW) operation of these LDs with high PCE at high power has made them favorable for industrial applications.

Pietrzak *et al* [18] reported a maximum PCE of 61% for the 808 nm single emitter LDs with 95 μm stripe width and 2.0 mm long laser cavity. In this study, the waveguide thickness was increased to reduce the overlap of optical mode with the highly doped cladding layers, and the waveguide doping was optimized resulting in reduced optical loss from 1.05 cm^{-1} to 0.87 cm^{-1}. Jenoptik attained a PCE of 53% at 50 °C compared with a PCE of 60% at 25 °C for 808 nm bars by employing a heat sink with low thermal resistance

* Authors to whom any correspondence should be addressed.

[19]. nLight Corporation reported single emitter broad area devices with high-temperature (HT) structure design [20]. These devices had a PCE of 56% at 25 °C, and it was reduced to around 50% at 60 °C. In 2016, Coherent Inc. reported a PCE of 63% for a single emitter achieving 9 W at 8 A with a 140 μm stripe width [14]. A 200 μm wide emitter (c-mount package) exhibited 61% maximum PCE and achieved 12.5 W at 11 A. The highest reported PCE of 808 nm single emitter LDs was 65% with 9 W output power [21]. In the last decade, there has been limited improvement and lack of a systematic study on the efficiency of these lasers. Additionally, PCE loss investigation at high temperatures has rarely been reported but it is essential to improve the HT characteristics of single emitter LDs.

Improving the laser output power and PCE has been the subject of intense research and many studies have been carried out to examine the causes of their limitations. The output power was considered to be deteriorated by many factors, such as free-carrier absorption [22], longitudinal spatial hole burning [23–26], two-photon absorption [24, 27], carrier leakage [22], and carrier non-pinning [28]. Novel designs have been introduced to mitigate these effects demonstrating 33 W continuous-wave [24] and 145 W pulsed output power [29] at room temperature for 100 μm wide GaAs-based LDs.

Various design approaches have been reported to improve the output power and efficiency based on the epitaxial design optimization [13, 30, 31]. To realize high electro-optical conversion efficiency with reliable operation, the development of semiconductor lasers should incorporate essential characteristics in epitaxial design, growth, and fabrication: (a) a high-efficiency design requires optimization for low optical losses and electrical resistance with high internal quantum efficiency. (b) A high-quality epitaxial growth with very low bulk material defect density. (c) Advanced processing and assembly capability that contains etching, ohmic contact, cleavage, facet passivation, and mirror coating. Besides, thermal management of the chip and laser facet temperature are significant factors for reliable operation of the LDs [32–34]. For high temperature stability and long-term reliable operation, the epitaxy and waveguide structures need to be designed by considering thermal effects as well.

This report compares the symmetric broad-area laser (S-BAL) with asymmetric broad-area laser (A-BAL) designs both theoretically and experimentally by investigating the power loss paths for 808 nm single-emitter lasers with 4 mm cavity length and 190 μm stripe width. A-BAL design shifts the optical field distribution toward the n-side to reduce optical losses, where the absorption cross-section is approximately three times smaller compared to the p-side. The PCE was increased from 60.4% to 66.3% at 10 W output power by using the A-BAL design at 25 °C. We analyzed the energy loss paths of the A-BAL under different temperature conditions. Carrier leakage was found to be the primary reason for the PCE reduction at higher temperatures. Finally, by optimizing the A-BAL design for lower carrier leakage loss, we obtained devices with a 68% PCE at 10 W and significantly improved temperature characteristics with a PCE of 60.4% at 75 °C. These devices demonstrated low far-field divergence angle, uniform luminous intensity and operated for 2000 h without catastrophic optical damage.

2. Epitaxial structure design and device fabrication

The PCE, η_c, for LDs can be written in terms of laser parameters as:

$$\eta_c = \eta_i \frac{h\nu}{q} \frac{I - I_{th}}{I(V_0 + IR_s)} \frac{\alpha_m}{\alpha_i + \alpha_m} \tag{1}$$

where η_i is the internal quantum efficiency, $h\nu$ is the photon energy, q is the electron charge, I_{th} is the threshold current, V_0 is the built-in voltage, R_s is the series resistance, α_m is the mirror loss, and α_i is the internal loss [35]. To enhance η_c of a laser structure, the following factors need to be considered: (a) improving the internal quantum efficiency by increasing the electron injection efficiency and reducing the carrier leakage. (b) Optimizing the doping and material composition to reduce the series resistance [36]. Series resistance can be induced by many different material junctions, such as the metal-semiconductor contact and the semiconductor heterojunctions. By careful material choices and appropriate doping concentration, lower series resistance can be obtained. (c) Diminishing the internal loss, including built-in electric field loss, Joule heat, optical absorption, and scattering losses. (d) Reducing the threshold current, which is mainly determined by the quantum confinement factor of the active region, internal loss, and internal quantum efficiency.

We systematically compared S-BAL and A-BAL designs both numerically and experimentally by designing both structure types as identical as possible. A 1.2 μm thick n-buffer GaAs with a doping concentration of 2×10^{18} cm^{-3} was grown on the Si-doped GaAs substrate. Next, $Al_{0.45}Ga_{0.55}As$ n-cladding with a doping concentration of 4×10^{17} cm^{-3} and the undoped $Al_{0.36}Ga_{0.64}As$ waveguide layers were grown. The active region comprises a compressively strained 7 nm thick InGaAlAs single quantum well (QW) sandwiched between $Al_{0.3}Ga_{0.7}As$ barrier layers. The barriers were designed to reduce the carrier leakage from the active region and increase the electron injection efficiency. In S-BAL, the waveguide was surrounded symmetrically by $Al_{0.45}Ga_{0.55}As$ cladding layers with a total thickness of 2.2 μm. For A-BAL, p-cladding is $Al_{0.7}Ga_{0.3}As$, and the QW position is shifted towards the p-cladding. The mobility of holes in the p-type layer is much lower than that of the electrons in the n-type layer (usually an order of magnitude smaller). Thus, appropriately increasing the doping concentration of the p-type layers can greatly reduce R_s of the device and increase PCE. Hence, a doping concentration of 3×10^{18} cm^{-3} was used for the p-cladding. The p-GaAs contact layer has a doping concentration of higher than 2×10^{19} cm^{-3} to create an ohmic contact. The so-called voltage defect (V_d) was minimized by designing graded interface layers and doping profiles.

Figure 1 illustrates the calculated profiles of the refractive index and the optical intensity of the fundamental vertical mode for both S-BAL and A-BAL epitaxial structure designs. Higher-order vertical modes are not demonstrated since the

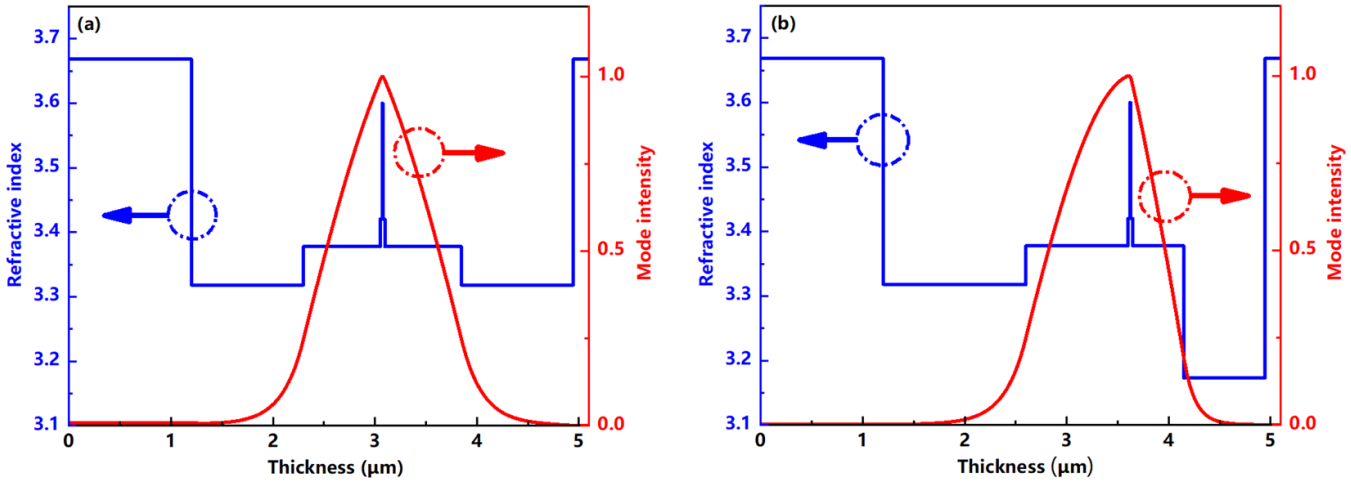

Figure 1. Refractive index and optical intensity (fundamental vertical mode) simulation results for (a) S-BAL and (b) A-BAL epitaxial designs.

Table 1. Confinement factor and optical absorption loss of different regions for S-BAL and A-BAL designs.

	S-BAL design		A-BAL design	
Region	Confinement factor	Absorption loss	Confinement factor	Absorption loss
p-cladding	0.8%	0.150 cm^{-1}	0.3%	0.093 cm^{-1}
p-waveguide	46.1%	0.111 cm^{-1}	25.2%	0.060 cm^{-1}
Barrier	2.6%	0.016 cm^{-1}	2.3%	0.014 cm^{-1}
QW	0.92%	0.294 cm^{-1}	0.84%	0.270 cm^{-1}
Barrier	2.6%	0.005 cm^{-1}	2.4%	0.005 cm^{-1}
n-waveguide	46.1%	0.037 cm^{-1}	68.2%	0.055 cm^{-1}
n-cladding	0.8%	0.013 cm^{-1}	0.8%	0.013 cm^{-1}
Total	100%	0.626 cm^{-1}	100%	0.510 cm^{-1}

waveguide does not support them for both designs. Compared with S-BAL, A-BAL adopted the refractive index asymmetric structure of the cladding layer through AlGaAs composition. In the A-BAL, the refractive index contrast of the p-cladding and p-waveguide is relatively larger, which causes the optical mode in the p-waveguide to shift towards the n-side and deviate from the original symmetric mode. As shown in figure 1(b), we also adopted the thickness asymmetric waveguide structure to reduce the interaction between hole carriers and optical mode in the waveguide. To evaluate the optical absorption loss for the designs, the optical confinement factor and loss of every epitaxial layer were calculated using the following equations:

$$\alpha_j = \Gamma_j(\sigma_n n_j + \sigma_p p_j) \tag{2}$$

$$\Gamma_j = \frac{\int_{j-1}^{j} |E|^2 dz}{\int |E|^2 dz} \tag{3}$$

where α_j and Γ_j are the optical absorption loss and confinement factor for the layer *j;* σ_n and σ_p are the free carrier absorption cross-section coefficients of electrons and holes; n_j and p_j are the carrier concentrations in the layer *j* of electrons and holes, respectively. The absorption cross-section coefficients for all compositions are assumed to be equal to that of the GaAs bulk material as $\sigma_n = 4 \times 10^{-18}$ cm^2 and $\sigma_p = 12 \times 10^{-18}$ cm^2, respectively [37]. The calculation results are based on the mode intensity and carrier concentrations distribution in different regions. For n- and p-claddings, the doping levels are set as the carrier concentration. The carrier concentration in the waveguides, barriers, and QW are assumed as 2×10^{16}, 5×10^{16}, and 2×10^{18} cm^{-3}, respectively. Table 1 presents the calculated confinement factor and absorption loss of epitaxial regions for both designs. The total absorption loss of p-waveguide and p-cladding was 0.261 cm^{-1}, which accounted for about 42% of the total loss for the S-BAL structure. However, the loss of p-region was reduced to 0.153 cm^{-1} and only make up about 30% of the total loss for the A-BAL structure. A-BAL design has a lower optical mode overlap with the high absorption loss p-doped region, resulting in reduced absorption losses.

Metal-organic chemical vapor deposition was used for epitaxial growth of the laser structures under optimized conditions. After the growth, a wet-chemical etching process was applied to form a ridge waveguide structure. A Si_3N_4 film was deposited as an insulating layer. A current injection region pattern was formed by selective etching of the Si_3N_4 film, and Ti/Pt/Au was evaporated as p-contact. After wafer thinning to 120 μm, AuGe/Ni/Au was deposited as an n-contact. Then, the wafer was cleaved into bars with cavity lengths of

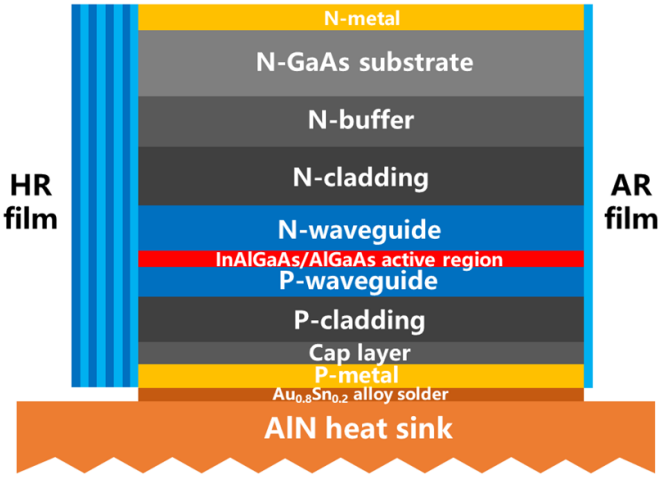

Figure 2. Schematic diagram of the 808 nm single emitter LDs.

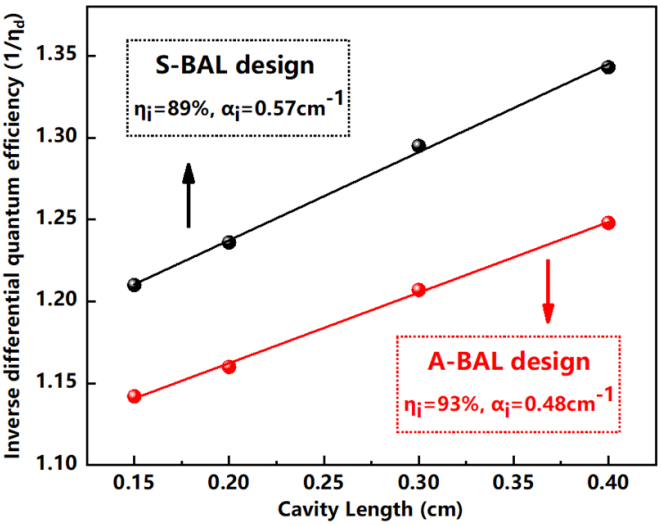

Figure 3. Dependence of inverse differential quantum efficiency on cavity length for 808 nm epitaxial wafer of both designs.

1.5, 2.0, 3.0, and 4.0 mm to characterize the internal quantum efficiency and the internal loss. For single emitter laser performance evaluation, 190 μm wide and 4.0 mm long cavity devices are employed. Subsequently, Ar plasma was applied for surface cleaning and a 5 nm thick Si film was deposited on the cleaved surface to prevent oxygen diffusion. Finally, high reflectivity (95%) and low reflectivity (2%) films were coated on the rear and front cavity surfaces, respectively. The bars were cleaved into single emitters and soldered on AlN heat sinks with $Au_{0.8}Sn_{0.2}$ as p-side down. Figure 2 illustrates the schematic of the device.

3. Results and discussion

3.1. Performance comparison for the two designs

First, uncoated bare devices with 100 μm stripe width and four different cavity lengths were investigated under pulsed operation with a low duty cycle (100 μs pulses with 100 Hz repetition) to extract the internal parameters of the epitaxial structure. The dependencies of the inverse differential quantum efficiency ($1/\eta_d$) on the cavity length (L) are shown in figure 3 for A-BAL and S-BAL designs, where each point represents the average data of five chips. By linear fitting of the results, the internal quantum efficiency (η_i) and internal optical loss (α_i) can be determined [17]. The internal quantum efficiency was 93%, and the internal optical loss was 0.48 cm^{-1} for the A-BAL device. Compared with S-BAL LDs, A-BAL demonstrates higher internal quantum efficiency and lower internal loss, which are crucial to achieving a high PCE. One would expect that α_i is lower for A-BAL design, as presented in table 1, because of the lower overlap with the p-side. The measured η_i is higher for A-BAL than S-BAL since a thinner p-waveguide should significantly reduce the voltage-driven carrier accumulation. The higher η_i and lower α_i lead to higher slope efficiency.

Figure 4 presents the electro-optical and spectral characteristics of 808 nm single emitter LDs for both designs. Measured threshold current, slope efficiency, operating voltage, and series resistance were 1.35 A, 1.31 W A^{-1}, 1.67 V, and 13.6 mΩ at 25 °C heatsink temperature for the A-BAL device. For 10 W output power at 25 °C, the A-BAL device achieves a PCE of 66.3%, while S-BAL can only reach a PCE of 60.4%. A slight rollover was observed for S-BAL above 9 A due to the excessive heat generation. The inset is the emission spectrum of an A-BAL at 10 W showing a center wavelength of around 808 nm at room temperature. The full width at half maximum (FWHM) of the spectrum was 1.3 nm and the full width at 90% of integrated power under the curve was 1.8 nm.

3.2. HT characteristics analysis for A-BAL

Figure 5 shows the temperature dependence of the light-current characteristics for the A-BAL device at heatsink temperatures varying from 25 °C to 75 °C. The variations of threshold current and slope efficiency with temperature are also displayed on the same graph. The device exhibited thermal rollover under high current and high temperature. The characteristic temperatures are significant parameters to evaluate thermal stability and lifetime of devices [38]. From the temperature-dependent threshold current and slope efficiency results, the characteristic temperature parameter T_0 was obtained as 155 K by fitting an exponential dependence of I_{th} on T to the experimental data. The characteristic temperature parameter T_1 of the slope efficiency was 311 K in the same temperature range. Figure 6 shows the electro-optical conversion efficiency versus current under different test temperatures for the S-BAL and A-BAL devices. For 10 W output power, the PCE reduces from 66.3% at 25 °C to 54.7% at 75 °C. Table 2 lists the specific parameters of the A-BAL devices under different test temperatures. Compared with the S-BAL device, the A-BAL device has 3%–5% higher PCE at

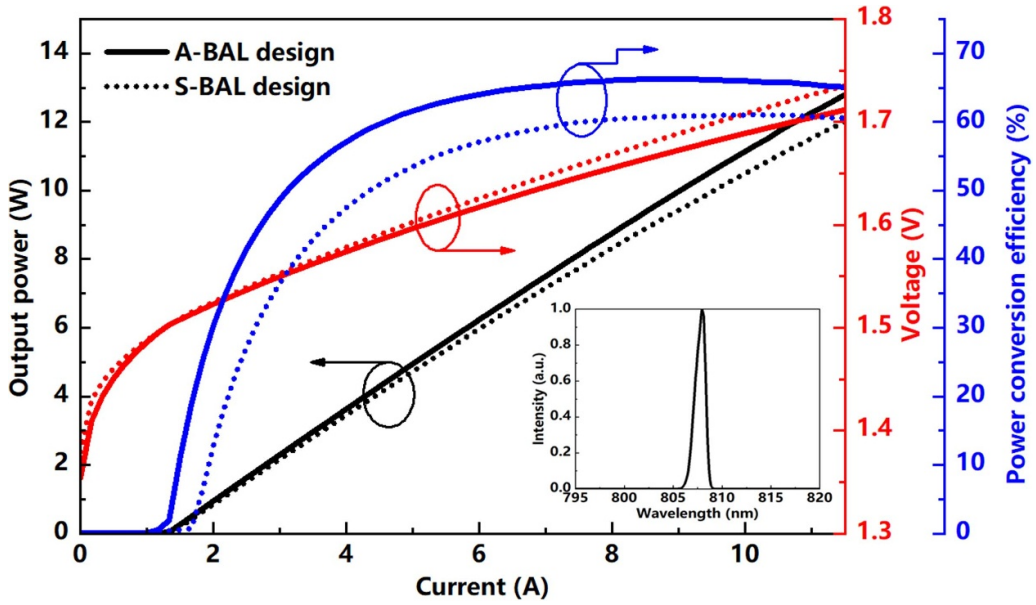

Figure 4. Electro-optical characteristics of 808 nm single emitter LDs with a 4 mm cavity length and 190 μm width for both designs. The inset is the corresponding spectra for an A-BAL device.

all temperatures, which shows its advantages. However, the significant reduction of PCE and apparent thermal rollover implies that the A-BAL device had poor temperature characteristics, which need to be improved. Figure 7 presents spectral data at different temperatures. The bandgap of the active region and the corresponding quasi-Fermi energy level difference decreases with temperature, resulting in a redshift of the emission wavelength. The calculated thermal drift coefficient is 0.304 nm $^{\circ}C^{-1}$ according to figure 7. The spectral FWHM is broadened from 1.2 nm to 2.0 nm with a temperature increase from 25 °C to 75 °C, possibly due to the heat accumulation effect and the uneven heat distribution in the active region.

Many mechanisms inside an LD consume the electrical input, and the paths of power loss can be analyzed to investigate the reasons for the performance degradation of an LD under HT conditions. The following equations can express the distribution of input power for the LDs

$$P_{\text{input}} = IV = I^2R_s + IV_0 \tag{4}$$

$$V_0 = V_d + V_F. \tag{5}$$

where V_0, V_d, and V_F represent the built-in voltage (i.e. given by the IV extrapolation to zero current in the linear region after turn-on), the voltage defect caused by the hetero-junction barriers, and quasi-Fermi level difference corresponding to the lasing energy, respectively [36]. A more detailed expression for P_{input} can be written according to the above equations as:

$$P_{\text{input}} = I^2R_s + IV_d + \eta_i I_{th} V_F + IV_F(1-\eta_i) + \eta_i(I-I_{th})V_F. \tag{6}$$

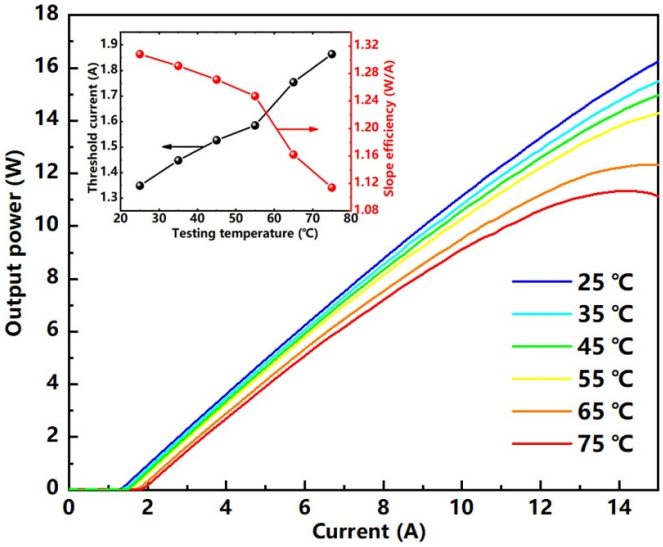

Figure 5. *L–I* characteristics of the A-BAL design at heatsink temperatures varying from 25 °C to 75 °C. The inset shows the variation of threshold current and slope efficiency with temperature. The lines in the inset are a guide for the eye.

The external differential quantum efficiency η_d has a relationship with η_i as:

$$\eta_d = \eta_i \frac{\alpha_m}{\alpha_i + \alpha_m} \tag{7}$$

$$\alpha_m = \frac{1}{2L} \ln\left(\frac{1}{R_1R_2}\right) \tag{8}$$

where α_i and α_m represent internal loss and mirror loss, respectively; L is the cavity length; R_1 and R_2 are the reflectivity of the front and rear facets, respectively. According to

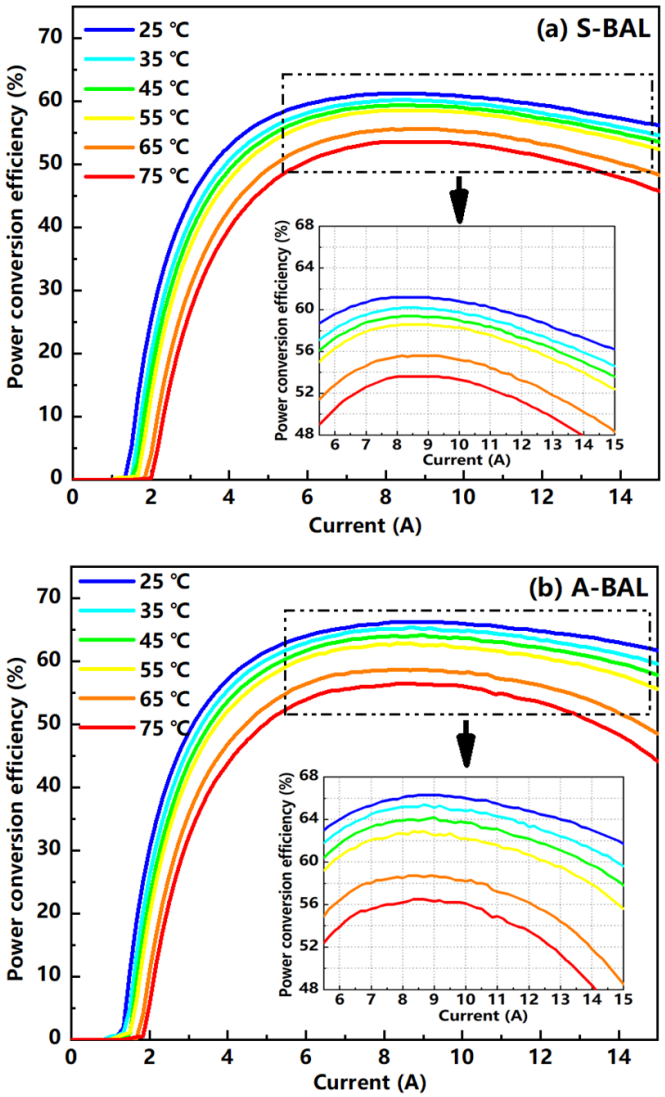

Figure 6. PCE versus current characteristics of the (a) S-BAL, and (b) A-BAL design at heatsink temperatures varying from 25 °C to 75 °C. The insets are partially enlarged pictures.

Table 2. The A-BAL device performance parameters at different testing temperatures for 10 W output power.

T (°C)	I_{th} (A)	S (W A^{-1})	V_{op} (V)	R_s (mΩ)	I_{op} (A)	λ_{center} (nm)	$\Delta\lambda_{FWHM}$ (nm)	PCE
25	1.349	1.308	1.673	13.6	9.02	808.3	1.15	66.3%
35	1.448	1.291	1.657	13.2	9.25	810.7	1.17	65.2%
45	1.527	1.271	1.653	13.2	9.47	813.2	1.30	63.9%
55	1.585	1.247	1.648	12.8	9.74	817.4	1.33	62.3%
65	1.754	1.162	1.643	12.2	10.50	820.1	1.80	57.9%
75	1.864	1.114	1.642	11.9	11.13	823.5	1.96	54.7%

equation (6), the input power can be classified into five parts to quantify the contribution of each mechanism:

(a) Joule heating loss of I^2R_s mainly comes from the ohmic contact and bulk resistance of the semiconductor.
(b) The voltage defect loss (i.e. built-in hetero-barrier loss) IV_d is mainly caused by misalignment of the heterojunctions.
(c) $\eta_i I_{th} V_F$ represents the power dissipated below the lasing threshold.
(d) The carrier leakage loss (i.e. carrier overflow loss) $IV_F(1 - \eta_i)$ results in voltage-driven accumulation and recombination of electrons and holes outside the QW.
(e) $\eta_i(I - I_{th})V_F$, is the stimulated emission term that includes the laser output, free carrier absorption, and scattering losses.

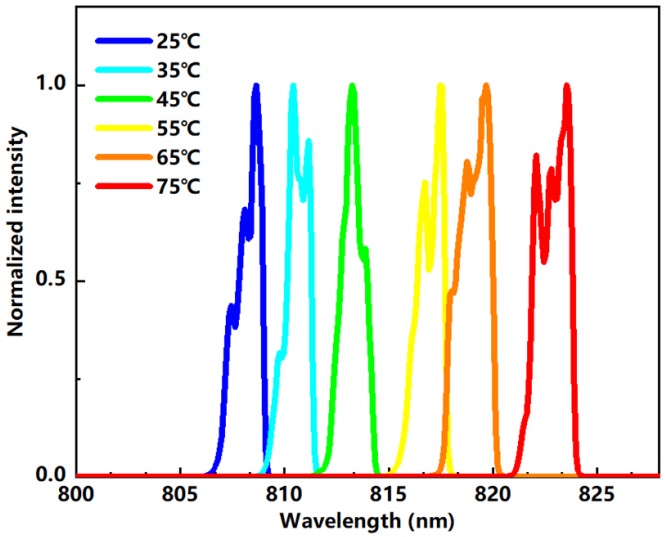

Figure 7. Spectral characteristics of the A-BAL design at heatsink temperatures varying from 25 °C to 75 °C.

Table 3. Comparison of power loss proportions at different temperatures for the A-BAL device at 10 A.

	Stimulated emission $(\eta_i(I - I_{th})V_F)$					
T (°C)	Output	Abs. & Scat.	Joule heating loss (I^2R_s)	Voltage defect loss (IV_d)	Below threshold $(\eta_i I_{th} V_F)$	Carrier leakage loss $(IV_F(1 - \eta_i))$
25	65.9%	6.0%	8.0%	1.3%	11.2%	7.6%
35	64.7%	5.7%	7.9%	0.6%	11.9%	9.2%
45	63.6%	5.3%	7.9%	0.5%	12.4%	10.2%
55	62.1%	4.9%	7.7%	0.6%	12.6%	12.1%
65	58.1%	4.4%	7.5%	0.3%	13.3%	16.6%
75	56.0%	3.9%	7.3%	0.3%	13.7%	18.8%

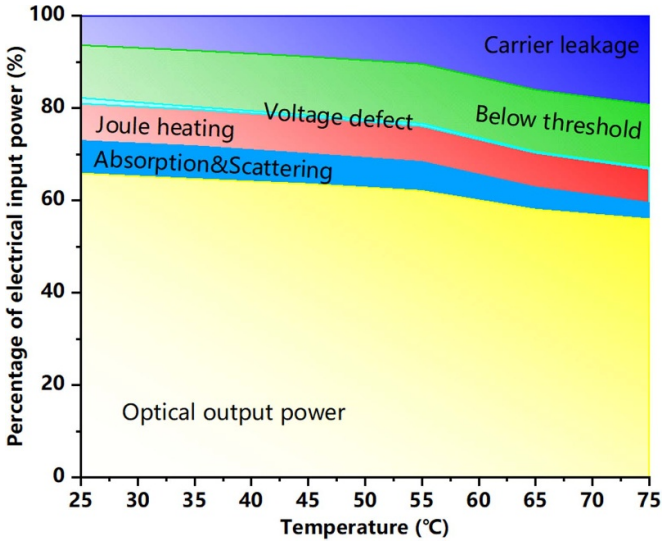

Figure 8. Temperature-dependent input power distribution of the 808 nm single emitter LD with A-BAL design at heatsink temperatures varying from 25 °C to 75 °C.

Table 3 presents the detailed values and figure 8 shows the distribution of different power loss types estimated according to equation (6) for the A-BAL single emitter at different heatsink temperatures. Among various loss mechanisms, the carrier leakage strongly dominates the heat-induced losses. The carrier leakage loss increased significantly from 7.6% at 25 °C to 18.8% at 75 °C, which was the primary reason for the PCE reduction. Besides, the increase of the threshold current with the test temperature is the reason for the increase in the proportion of power dissipated below the lasing threshold.

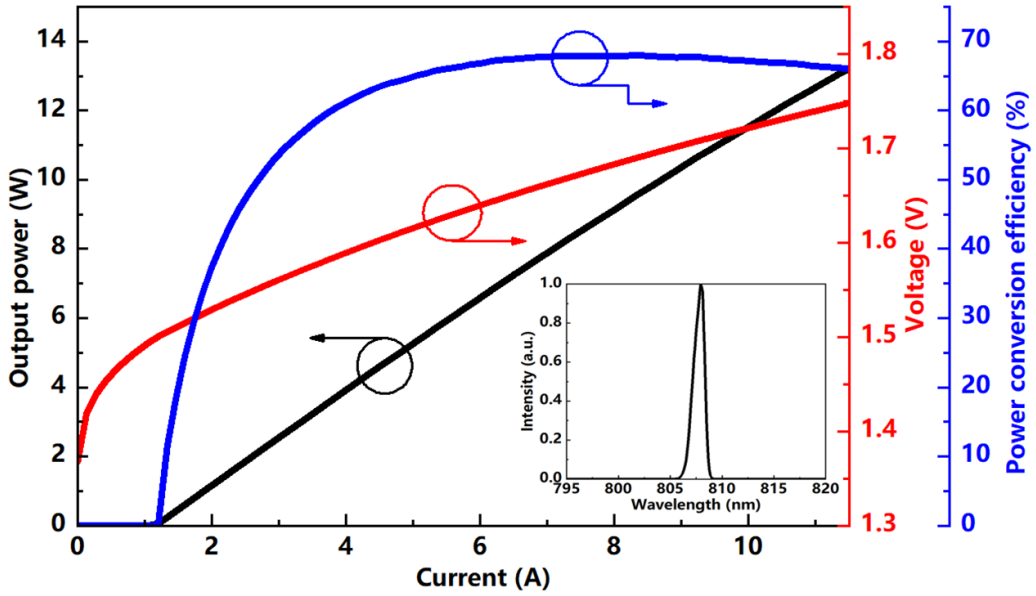

Figure 9. The *L–I–V*, and spectral characteristics of 808 nm single emitter LD with the optimized A-BAL design at 25 °C.

The low voltage defect loss confirms the high quality of epitaxial material growth, especially for the hetero-junction barriers.

3.3. A-BAL-optimized design for improved temperature characteristics

The challenge is to obtain high PCE at high heatsink temperatures. Our approach was to increase the carrier confinement and suppression of carrier leakage by increasing the waveguide bandgap, although it sacrifices the series resistance. To improve A-BAL devices' temperature characteristics, we increased the aluminum composition of the p- and n-waveguide by 2%. Hence, the bandgap difference between the active region and the waveguide increases, leading to enhanced carrier confinement in the active region at high temperatures. The significantly reduced carrier leakage compensated for the increase in series resistance. Figure 9 shows the *L–I* and *V–I* characteristics of an 808 nm single emitter LD with the optimized A-BAL design. The PCE at 10 W was 68%, which is a record high value for 808 nm single emitter LDs at room temperature. The threshold current, operating voltage, series resistance, and slope efficiency were 1.19 A, 1.70 V, 19.3 mΩ, and 1.35 W A^{-1}. The inset shows the lasing spectrum with a center wavelength of 808 nm and a spectral FWHM of 1.2 nm.

To understand the temperature-dependent behavior of the performance for the optimized A-BAL, figure 10 shows the CW PCE–*I* and *L–I* characteristics at heatsink temperatures from 25 °C to 75 °C. The A-BAL-optimized device delivers a much higher PCE of 60.4% compared with 54.7% of the A-BAL for optical power of 10 W at 75 °C. The improved temperature characteristics are mainly due to the increase in the Al composition of the waveguide layer, which reduces the escape of hot carriers from the QW. The leakage of carriers becomes more severe at higher

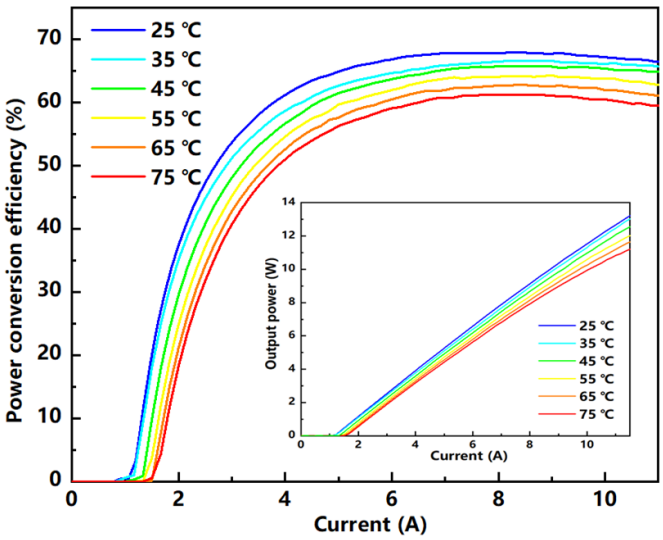

Figure 10. PCE versus current characteristics of the 808 nm single emitter LD with the A-BAL-optimized design at heatsink temperatures varying from 25 °C to 75 °C. The inset is the *L–I* curve of the laser.

temperatures. However, A-BAL-optimized design suppresses the temperature-dependent performance degradation strongly compared to the A-BAL design as figure 11 shows in more detail. Figure 11 compares the measured temperature dependence of threshold current and slope efficiency for the A-BAL and A-BAL-optimized LDs. The A-BAL-optimized laser had distinctly better characteristics with lower threshold current and higher slope efficiency at all temperatures. The improvement in these parameters is even more considerable at higher temperatures consistent with expectations and PCE results. The improved temperature behavior of A-BAL-optimized indicates its suitability for HT operation and promising for a longer lifetime.

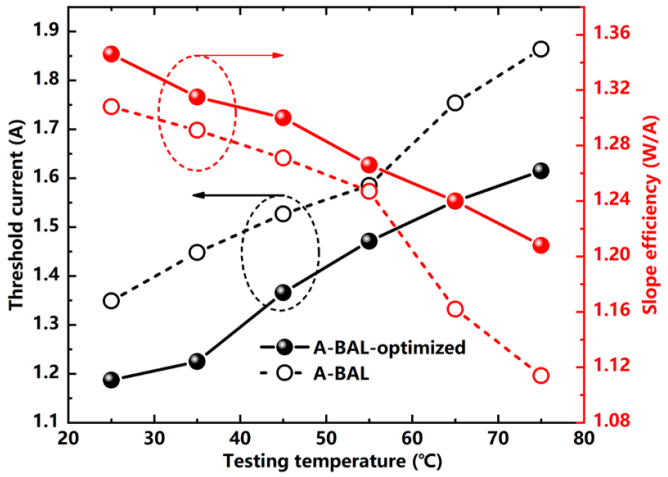

Figure 11. Threshold current and slope efficiency comparison for the 808 nm single emitter LD with the A-BAL and A-BAL-optimized design at heatsink temperatures from 25 °C to 75 °C.

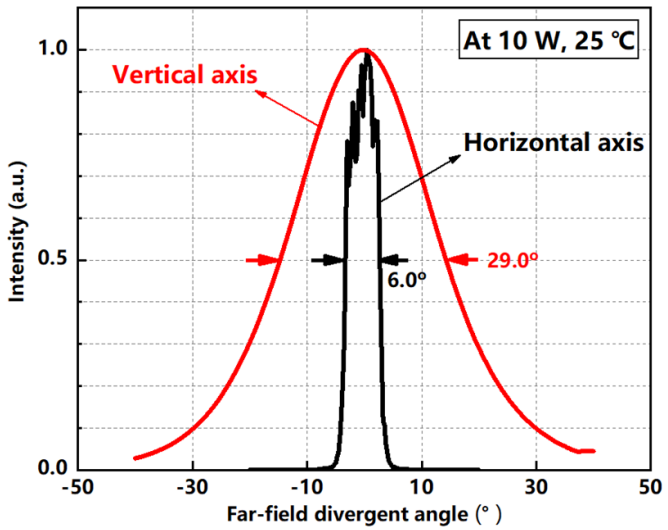

Figure 12. Far-field profiles of A-BAL-optimized at 10 W and 25 °C.

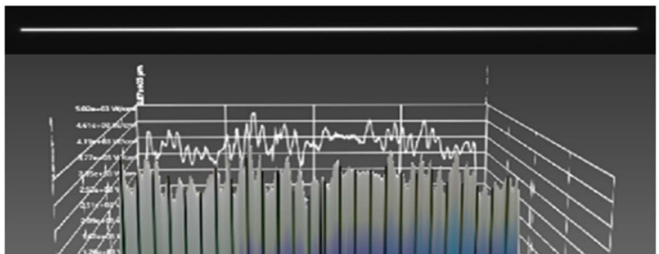

Figure 13. Near-field light intensity distribution of a typical A-BAL-optimized device. The top figure shows the corresponding electroluminescence appearance pictured by an infrared microscope.

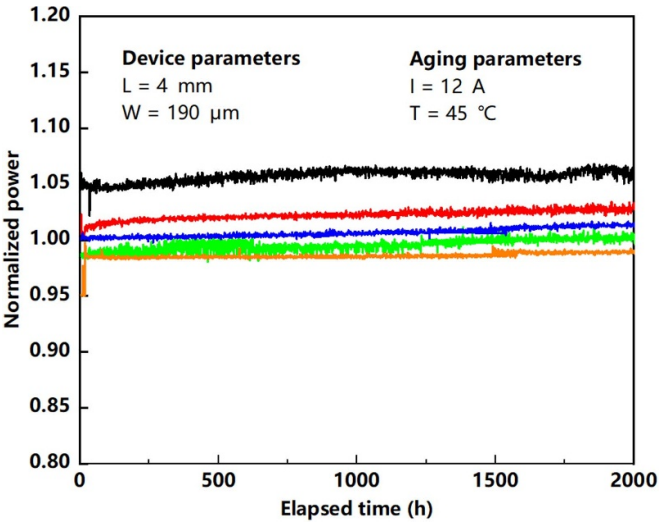

Figure 14. Accelerated lifetime test for the 808 nm A-BAL-optimized single emitter devices.

The far-field profiles of the A-BAL-optimized are shown in figure 12. The FWHM of the horizontal and vertical axes are 6.0° and 29.0° at 10 W, respectively. There are some lobes in the far-field distribution of the horizontal axis due to the high number of lateral optical modes. In agreement with figure 1(b), the large optical cavity structure with a single vertical optical mode leads to diffraction-limited far-field in the vertical axis. Figure 13 is the near-field profile and luminous intensity distribution of a typical A-BAL-optimized device under 0.9 times operating current. The intensity height represents the relative power density (W cm^{-2}) received by the CCD pixels at different luminous positions, showing a fairly uniform profile.

We carried out life tests to confirm the reliable long-term operation since reliability is essential for high power LDs. Five chip-on-submounts have been included in the accelerated lifetime test under a constant injection current of 12 A at a heatsink temperature of 45 °C. The output power is 13 W, and the junction temperature is estimated to be 70 °C. Figure 14 shows the variation of normalized power as a function of accelerated aging time. These devices have been operating for 2000 h, and no wear-out behavior has been observed. The accelerated life test results show the long-term reliability of the epitaxial design, growth, and process technology.

4. Conclusion

We compared S-BAL and A-BAL epitaxial designs both theoretically and experimentally for 808 nm single emitter LDs. A lower optical absorption loss and higher internal quantum efficiency of the A-BAL structure resulted in a higher PCE of 66.3% for 10 W output power at 25 °C, compared to 60.4% for the S-BAL design. By analyzing the A-BAL device output

characteristics, carrier leakage was found to be the dominating loss mechanism for PCE degradation at high temperatures. By optimizing the carrier confinement, carrier leakage at high temperatures was suppressed strongly. As a result, a record-high 808 nm laser single-emitter PCE of 68% at 25 °C and 60.4% at 75 °C was achieved for 10 W output power demonstrating their suitability for HT applications. 2000 h of accelerated life testing has been completed without any failure demonstrating the high reliability of these devices.

Data availability statement

The data that support the findings of this study are available upon reasonable request from the authors.

Acknowledgments

This work was supported by Project of Xi'an Institute of Optics and Precision Mechanics, Chinese Academy of Sciences No. Y855J61213, National Natural Science Foundation of China under Grant No. 61504167, and the Natural Science Foundation of Shaanxi Province No. 2015JQ6263.

ORCID iD

Abdullah Demir https://orcid.org/0000-0003-4678-0084

References

[1] Bachmann F G and Russek U A 2002 Laser welding of polymers using high-power diode lasers *Photon Processing in Microelectronics and Photonics* vol 4637 (Bellingham, WA: International Society for Optics and Photonics) (https://doi.org/10.1117/12.515630)
[2] Bachmann F 2003 Industrial applications of high power diode lasers in materials processing *Appl. Surf. Sci.* **208** 125–36
[3] Urata Y and Wada S 2005 808 nm diode-pumped continuous-wave Tm: $gdVO_4$ laser at room temperature *Appl. Opt.* **44** 3087–92
[4] Chen F, Yu X, Gao J, Li X D, Zhang Z, Yan R P, Yu J H and Zhang Z H 2008 Efficient generation of 914 nm laser with high beam quality in Nd: YVO4 crystal pumped by π-polarized 808 nm diode-laser *Laser Phys. Lett.* **5** 655–8
[5] Tian Y, Wei T, Cai M, Chen F, Wang F, Jing X, Zhang J, Zhang Q and Xu S 2014 Enhancement of 1.53 μm emission in erbium/cerium-doped germanosilicate glass pumped by common 808 nm laser diode *Appl. Opt.* **53** 6148–54
[6] Li Y-H, Kang Z-L and Hu L-M 2010 New application of semiconductor laser in medical field *Laser J.* **31** 73–5
[7] Lepselter J and Elman M 2004 Biological and clinical aspects in laser hair removal *J. Dermatol. Treat.* **15** 72–83
[8] Wang J, Smith B, Xie X, Wang X and Burnham G T 1999 High-efficiency diode lasers at high output power *Appl. Phys. Lett.* **74** 1525–7
[9] Yang G, Smith G M, Davis M K, Kussmaul A, Loeber D A S, Hu M H, Nguyen H-K, Zah C-E and Bhat R 2004 High-performance 980 nm ridge waveguide lasers with a nearly circular beam *IEEE Photonics Technol. Lett.* **16** 981–3
[10] Gapontsev V *et al* 2008 8xx–10xx nm highly efficient single emitter pumps *High-Power Diode Laser Technology and Applications VI* vol 6876 (Bellingham, WA: International Society for Optics and Photonics) (https://doi.org/10.1117/12.763999)
[11] Gapontsev V *et al* 2009 High-brightness fiber coupled pumps *High-Power Diode Laser Technology and Applications VII* vol 7198 (Bellingham, WA: International Society for Optics and Photonics) (https://doi.org/10.1117/12.809456)
[12] Bao L *et al* 2010 Reliability of high performance 9xx nm single emitter laser diodes *High-Power Diode Laser Technology and Applications VIII* vol 7583 (Bellingham, WA: International Society for Optics and Photonics) (https://doi.org/10.1117/12.842856)
[13] Crump P *et al* 2013 Efficient high-power laser diodes *IEEE J. Sel. Top. Quantum Electron.* **19** 1501211
[14] Morales J *et al* 2016 Advances in 808 nm high power diode laser bars and single emitters *High-Power Diode Laser Technology and Applications XIV* vol 9733 (Bellingham, WA: International Society for Optics and Photonics) (https://doi.org/10.1117/12.2213789)
[15] Gao W *et al* 2007 High-power highly reliable single emitter laser diodes at 808 nm *High-Power Diode Laser Technology and Applications V* vol 6456 (Bellingham, WA: International Society for Optics and Photonics) (https://doi.org/10.1117/12.701612)
[16] Abbasi S P and Mahdieh M H 2017 Asymmetric, nonbroadened waveguide structures for double QW high-power 808 nm diode laser *XXI Int. Symp. on High Power Laser Systems and Applications 2016* vol 10254 (International Society for Optics and Photonics) (https://doi.org/10.1117/12.2257308)
[17] Wang Z, Li T, Yang G and Song Y 2017 High power, high efficiency continuous-wave 808 nm laser diode arrays *Opt. Laser Technol.* **97** 297–301
[18] Pietrzak A *et al* 2016 High-power single emitters and low fill factor bars emitting at 808 nm *High-Power Diode Laser Technology and Applications XIV* vol 9733 (Bellingham, WA: International Society for Optics and Photonics) (https://doi.org/10.1117/12.2212709)
[19] Schröder D *et al* 2009 Improved laser diode for high power and high temperature applications *High-Power Diode Laser Technology and Applications VII* vol 7198 (Bellingham, WA: International Society for Optics and Photonics) (https://doi.org/10.1117/12.809997)
[20] Wang J *et al* 2010 Reliability and performance of 808 nm single emitter multi-mode laser diodes *High-Power Diode Laser Technology and Applications VIII* vol 7583 (Bellingham, WA: International Society for Optics and Photonics) (https://doi.org/10.1117/12.842876)
[21] Bao L *et al* 2012 High performance diode lasers emitting at 780–820 nm *High-Power Diode Laser Technology and Applications X* vol 8241 (Bellingham, WA: International Society for Optics and Photonics) (https://doi.org/10.1117/12.910321)
[22] Piprek J and Zhan-Ming L 2018 What causes the pulse power saturation of GaAs-based broad-area lasers? *IEEE Photonics Technol. Lett.* **30** 963–6
[23] Demir A *et al* 2015 29.5 W continuous wave output from 100 μm wide laser diode *High-Power Diode Laser Technology and Applications XIII* vol 9348 (Bellingham, WA: International Society for Optics and Photonics) (https://doi.org/10.1117/12.2077342)
[24] Demir A, Peters M, Duesterberg R, Rossin V and Zucker E 2015 Semiconductor laser power enhancement by control of gain and power profiles *IEEE Photonics Technol. Lett.* **27** 2178–81
[25] Wenzel H, Crump P, Pietrzak A, Wang X, Erbert G and Tränkle G 2010 Theoretical and experimental investigations of the limits to the maximum output power of laser diodes *New J. Phys.* **12** 085007

[26] Avrutin E A and Ryvkin B S 2019 Effect of spatial hole burning on output characteristics of high power edge emitting semiconductor lasers: a universal analytical estimate and numerical analysis *J. Appl. Phys.* **125** 023108
[27] Avrutin E A and Ryvkin B S 2016 Theory of direct and indirect effect of two-photon absorption on nonlinear optical losses in high power semiconductor lasers *Semicond. Sci. Technol.* **32** 015004
[28] Kaul T, Erbert G, Klehr A, Maasdorf A, Martin D and Crump P 2019 Impact of carrier nonpinning effect on thermal power saturation in GaAs-based high power diode lasers *IEEE J. Sel. Top. Quantum Electron.* **25** 1–10
[29] Tarasov I S *et al* 2007 High power CW (16 W) and pulse (145 W) laser diodes based on quantum well heterostructures *Spectrochim. Acta* A **66** 819–23
[30] Hasler K H, Wenzel H, Crump P, Knigge S, Maasdorf A, Platz R, Staske R and Erbert G 2014 Comparative theoretical and experimental studies of two designs of high-power diode lasers *Semicond. Sci. Technol.* **29** 045010
[31] Malag A, Dabrowska E, Teodorczyk M, Sobczak G, Kozlowska A and Kalbarczyk J 2012 Asymmetric heterostructure with reduced distance from active region to heatsink for 810 nm range high-power laser diodes *IEEE J. Quantum Electron.* **48** 465–71
[32] Tomm J W, Ziegler M, Hempel M and Elsaesser T 2011 Mechanisms and fast kinetics of the catastrophic optical damage (COD) in GaAs-based diode lasers *Laser Photonics Rev.* **5** 422–41
[33] Arslan S, Gundogdu S, Demir A and Aydınlı A 2019 Facet cooling in high power InGaAs/AlGaAs lasers *IEEE Photonics Technol. Lett.* **31** 94
[34] Demir A, Arslan S, Gündogdu S and Aydinli A 2019 Reduced facet temperature in semiconductor lasers using electrically pumped windows *Proc. SPIE* **10900** 109000R
[35] Bour D P and Rosen A 1989 Optimum cavity length for high conversion efficiency quantum well diode lasers *J. Appl. Phys.* **66** 2813–8
[36] Kanskar M *et al* 2005 High-power conversion efficiency Al-free diode lasers for pumping high-power solid-state laser systems *Novel In-Plane Semiconductor Lasers IV* vol 5738 (Bellingham, WA: International Society for Optics and Photonics) (https://doi.org/10.1117/12.597097)
[37] Kaul T, Erbert G, Maaßdorf A, Knigge S and Crump P 2018 Suppressed power saturation due to optimized optical confinement in 9xx nm high-power diode lasers that use extreme double asymmetric vertical designs *Semicond. Sci. Technol.* **33** 035005
[38] Świetlik T *et al* 2006 Anomalous temperature characteristics of single wide quantum well InGaN laser diode *Appl. Phys. Lett.* **88** 071121